Attitude Control by means of Explicit Model Predictive Control, via Multi-parametric Quadratic Programming

Øyvind Hegrenæs*[♯] Jan Tommy Gravdahl*[†] Petter Tøndel*[‡]

*Department of Engineering Cybernetics,
Norwegian University of Science and Technology
7491 Trondheim, Norway

***Abstract*— Explicit solutions to constrained linear MPC problems can be computed by solving multi-parametric quadratic programs (mpQP), where the parameters are the components of the state vector. The solution to the mpQP is a piecewise affine (PWA) function, which can be evaluated at each sample to obtain the optimal control law. The on-line computation effort is restricted to a table-lookup, and the controller can be implemented on inexpensive hardware as fixed-point arithmetics can be used. This is highly desirable for systems with limited power and CPU resources. An example of such systems is micro-satellites, which is the focus of this paper. In particular, the explicit MPC (eMPC) approach is applied to the SSETI/ESEO micro-satellite project, initiated by the European Space Agency (ESA). The theoretical results are supported by simulations.**

I. INTRODUCTION

The purpose of this paper is twofold. First, we establish a nonlinear model of a micro-satellite, with thrusters and a reaction wheel as actuators. Secondly, we propose a strategy to solve the attitude control problem for this satellite.

However, unlike preceding work, typically carried out using PD- or LQ-control [12], Lyapunov design procedures [2]-[3], sliding mode [4]-[5], adaptive- or quaternion feedback techniques [6]-[8], $\mathcal{H}_\infty$ or $\mathcal{H}_2/\mathcal{H}_\infty$ [9]-[11], the focus of this paper will be on explicit Model Predictive Control. This approach is shown to be a highly potential scheme, which should be considered if constraints need to be taken into account, while real-time optimization is impossible due to computational limitations. To the best knowledge of the authors, this approach has not yet been applied to attitude control of spacecrafts.

Stability proofs are not considered at this point. A potential approach is to search for piecewise quadratic Lyapunov functions by solving a convex optimization problem. In [13] this was done using linear matrix inequalities (LMIs).

When implementing the solution, an important thing to keep in mind is that the actuating thrusters are on-off by nature. A bang-bang modulation scheme with dead-zone will be utilized to address this problem.

The structural data and satellite model is based on the SSETI micro-satellite project, initiated by ESA.

The results in this paper are based on the work in [1].

[♯]Graduate student, e-mail: hegrenas@unik.no
[†]Associate Professor, e-mail: tommy.gravdahl@itk.ntnu.no
[‡]Postdoctoral Fellow, e-mail: petter.tondel@itk.ntnu.no

A. Explicit Model Predictive Control

When solving an MPC problem the control action, or equally, the solution, is obtained by computing an open-loop optimal sequence of control inputs on a predefined horizon, once for each time sample. The first control input in the sequence is then applied to the plant, and the optimization is repeated with the new initial conditions and on the new horizon, shifted one step ahead. Due to the shifted horizon, the term *receding horizon control* is commonly used interchangeably with MPC. For the remainder of this section, the process to be controlled can be described by a *discrete-time*, deterministic linear state-space model, that is

$$\begin{aligned} \mathbf{x}(k+1) &= \mathbf{A}\mathbf{x}(k) + \mathbf{B}\mathbf{u}(k) \\ \mathbf{y}(k) &= \mathbf{C}\mathbf{x}(k), \end{aligned} \tag{1}$$

where $\mathbf{x}(k) \in \mathbb{R}^n$ is the state variable, $\mathbf{u}(k) \in \mathbb{R}^m$ is the input variable, $\mathbf{A} \in \mathbb{R}^{n\times n}$, $\mathbf{B} \in \mathbb{R}^{m\times m}$, and $(\mathbf{A}, \mathbf{B})$ is a stabilizable pair. If we now consider the regulator problem, that is, the problem of driving the state vector to the origin, the traditional MPC solves the following optimization problem for the current $\mathbf{x}(k)$

$$\begin{aligned} &\min_{\mathbf{U},\mathbf{s}} \left\{ \mathcal{J}\left(\mathbf{U}, \mathbf{s}, \mathbf{x}(k)\right) \right\} \quad \text{subject to:} \\ &\mathbf{y}_{\min} - \mathbf{s} \leq \mathbf{y}_{k+i|k} \leq \mathbf{y}_{\max} + \mathbf{s},\ i = 1, \ldots, N \\ &\mathbf{u}_{\min} \leq \mathbf{u}_{k+i} \leq \mathbf{u}_{\max},\ i = 1, \ldots, M-1 \\ &\mathbf{u}_{k+i} = \mathbf{K}\mathbf{x}_{k+i|k},\ M \leq i \leq N-1 \\ &\mathbf{x}_{k|k} = \mathbf{x}(k) \\ &\mathbf{x}_{k+i+1|k} = \mathbf{A}\mathbf{x}_{k+i|k} + \mathbf{B}\mathbf{u}_{k+i},\ i \geq 0 \\ &\mathbf{y}_{k+i} = \mathbf{C}\mathbf{x}_{k+i|k},\ i \geq 0 \end{aligned} \tag{2}$$

where the cost function we seek to minimize is given as

$$\begin{aligned} \mathcal{J} = &\boldsymbol{\rho}\|\mathbf{s}\|_2^2 + \mathbf{x}_{k+N|k}^{\mathrm{T}}\mathbf{P}\mathbf{x}_{k+N|k} \\ &+ \Sigma_{i=0}^{N-1}\left\{\mathbf{x}_{k+i|k}^{\mathrm{T}}\mathbf{Q}\mathbf{x}_{k+i|k} + \mathbf{u}_{k+i}^{\mathrm{T}}\mathbf{R}\mathbf{u}_{k+i}\right\}, \end{aligned} \tag{3}$$

and $\mathbf{U} \triangleq [\mathbf{u}_k^{\mathrm{T}}, \ldots, \mathbf{u}_{k+M-1}^{\mathrm{T}}]^{\mathrm{T}}$, $\mathbf{s} \triangleq \left[\mathbf{s}_k^{\mathrm{T}}, \ldots, \mathbf{s}_{k+N-1}^{\mathrm{T}}\right]^{\mathrm{T}}$, $\mathbf{R} = \mathbf{R}^{\mathrm{T}} > 0$, $\mathbf{Q} = \mathbf{Q}^{\mathrm{T}} \geq 0$, $\mathbf{P} = \mathbf{P}^{\mathrm{T}} > 0$, $\mathbf{x}_{k+i|k}$ is the prediction of $\mathbf{x}(k+i)$ at time k, M and N are input and constraint horizons. When the final cost matrix $\mathbf{P}$ and gain matrix $\mathbf{K}$ are calculated from the algebraic Riccati equation, under the assumptions that the constraints are not active for $i \geq M$ and $i \geq N$, (2) exactly solves the constrained infinite horizon LQR problem for (1),

with weight matrices $\mathbf{R}$ and $\mathbf{Q}$. The additional variable $\mathbf{s} \in \mathbb{R}^{n_s}$ is a vector containing slack variables, while the term $\|\mathbf{s}\|_2$ is the $\mathcal{L}_2$-norm of $\mathbf{s}$, and $\boldsymbol{\rho}$ is the penalty weight of the slack variables. Note that using the $\mathcal{L}_2$-norm is only one way of including slack variables. The slack variables are defined in such a way that they are nonzero only if the output constraints are violated, yet heavily penalized in the cost function, so that the optimizer has a strong incentive to keep them zero if possible. If we have $\boldsymbol{\rho} = \boldsymbol{\infty}$, or equally $\mathbf{s} = \mathbf{0}$, the MPC problem in (2) obtains its most simple form, only involving *hard* constraints. For some applications the latter is the only applicable, e.g. physical limitations of components or saturation in actuation. The consequence of including hard constraints is that infeasibility may occur. This can for instance be the case if initial conditions are infeasible, if noise causes the output to go outside the feasible solution space in the next time step, or if there are serious model uncertainties. Obviously, this needs to be addressed in real applications, where the introduction of slack variables is one possibility.

1) From linear MPC to mpQP: It is shown in [14], with $\boldsymbol{\rho} = \boldsymbol{\infty}$, that the MPC problem (2) can be reformulated as

$$\begin{aligned} V_z(\mathbf{x}(k)) = \min_{\mathbf{z}} \left\{ \frac{1}{2}\mathbf{z}^{\mathrm{T}}\mathbf{H}\mathbf{z} \right\} \\ \text{subject to:} \quad \mathbf{G}\mathbf{z} \leq \mathbf{W} + \mathbf{S}\mathbf{x}(k), \end{aligned} \tag{4}$$

where $\mathbf{z} \triangleq \mathbf{U} + \mathbf{H}^{-1}\mathbf{F}^{\mathrm{T}}\mathbf{x}(k)$, $\mathbf{U}$ is defined as in (2), and $\mathbf{x}(k)$ is the current state, which can be treated as a vector of parameters. We have that $\mathbf{z} \in \mathbb{R}^{n_z}$, $\mathbf{H} \in \mathbb{R}^{n_z \times n_z}$, $\mathbf{G} \in \mathbb{R}^{q \times n_z}$, $\mathbf{W} \in \mathbb{R}^{q \times 1}$, and $\mathbf{S} \in \mathbb{R}^{q \times n}$. Note that $\mathbf{H} > 0$ since $\mathbf{R} > 0$. This is a strong result, as the problem formulated in (4) is strictly convex, and the Karush-Kuhn-Tucker (KKT) conditions are necessary and sufficient conditions for optimality, giving an unique solution.

As shown in [14], the mpQP in (4) can be solved by applying the KKT conditions

$$\begin{aligned} \mathbf{H}\mathbf{z} + \mathbf{G}^{\mathrm{T}}\lambda = 0, \quad \lambda \in \mathbb{R}^q, \\ \lambda_r \left(\mathbf{G}^r\mathbf{z} - \mathbf{W}^r - \mathbf{S}^r\mathbf{x}(k) \right) = 0, \quad r = 1, \ldots, q, \\ \lambda \geq 0, \\ \mathbf{G}\mathbf{z} - \mathbf{W} - \mathbf{S}\mathbf{x}(k) \leq 0, \end{aligned} \tag{5}$$

where the superscript r on a matrix denotes the r^{th} row, while q is the number of inequalities in the optimization problem. The number of *free variables* is $n_z = m \cdot N$.

A key observation is that (4) is solved explicitly for all $\mathbf{x}$. It is shown in [14] that the solution $\mathbf{z}^*(\mathbf{x}(k))$, hence $\mathbf{U}^*(\mathbf{x}(k))$, is a continuous piecewise affine (PWA) function defined over a polyhedra partition. Consequently, the on-line effort is limited to evaluating this PWA function.

Even though not derived for the case of including slack variables, both (4) and (5) can easily be extended to cover this situation, by defining the augmenting matrices $\widetilde{\mathbf{H}} \in \mathbb{R}^{\tilde{n}_z \times \tilde{n}_z}$, $\widetilde{\mathbf{G}} \in \mathbb{R}^{q \times \tilde{n}_z}$, and $\tilde{\mathbf{z}} \triangleq [\mathbf{z}, \mathbf{s}]^{\mathrm{T}} \in \mathbb{R}^{\tilde{n}_z}$. The number of free variables now becomes $\tilde{n}_z = n_z + n_s$.

B. SSETI/ESEO

The Student Space Exploration & Technology Initiative (SSETI) comprises several satellite projects. The specific satellite to be studied in this paper is the European Student Earth Orbiter (ESEO). Through the project, students from different European universities participate in designing, building and operating a micro-satellite. In addition to the satellite, the project includes the payload carried by the spacecraft and the associated ground systems. A short summary of structural data is given in Table I.

TABLE I
SSETI/ESEO PARAMETERS

Parameter	Value
Satellite inertia matrix, $\mathbf{I}$	$\mathrm{diag}(4.250, 4.337, 3.664)$ [kg m^2]
Axial wheel inertia, I_s	$4 \cdot 10^{-5}$ [kg m^2]
Axial wheel placement, $\mathbf{\Lambda}$	$[0, 1, 0]^{\mathrm{T}}$
Nominal thruster torque, $\mathbf{K}_{nom}$	$[0.0484, 0.0484, 0.0398]^{\mathrm{T}}$ [Nm]
Maximum applied wheel torque	0.0020 [Nm]
Maximum wheel velocity	527 [rad/s] $\approx$ 5032 rpm

II. MODELLING

In this section, a model describing a satellite with thrusters and a L-wheel cluster is derived. The notation is based on [16] and [17].

A. Kinematics

Due to their nonsingular parametrization, the Euler parameters are chosen to represent the kinematics. The Euler parameters are defined in terms of the angle-axis parameters θ and $\mathbf{k}$, and the mapping is defined as

$$\eta = \cos\frac{\theta}{2}, \quad \boldsymbol{\epsilon} = \mathbf{k}\sin\frac{\theta}{2} \tag{6}$$

which gives the corresponding rotation matrix

$$\mathbf{R}(\eta, \boldsymbol{\epsilon}) = \mathbf{1} + 2\eta\boldsymbol{\epsilon}^{\times} + 2\boldsymbol{\epsilon}^{\times}\boldsymbol{\epsilon}^{\times}. \tag{7}$$

From the properties of the rotation matrix, it can be shown that

$$\dot{\mathbf{R}}_o^b = \left(\boldsymbol{\omega}_{bo}^b\right)^{\times}\mathbf{R}_o^b = -\left(\boldsymbol{\omega}_{ob}^b\right)^{\times}\mathbf{R}_o^b \tag{8}$$

where $\boldsymbol{\omega}_{ob}^b$ is defined as the angular velocity of the body frame $\mathcal{F}_b$ relative the orbit frame $\mathcal{F}_o$, measured in $\mathcal{F}_b$, and $\mathbf{R}_o^b$ is the rotation matrix from $\mathcal{F}_b$ to $\mathcal{F}_o$. The orbit frame has its origin located at the center of mass of the satellite. Its z-axis is always nadir pointing (towards the center of Earth), while its x-axis is pointing in the direction of the forward velocity. The y-axis completes a right-hand coordinate system. From (7) and (8), the kinematic differential equations can be found as

$$\dot{\eta} = -\frac{1}{2}\boldsymbol{\epsilon}^{\mathrm{T}}\boldsymbol{\omega}_{ob}^b \tag{9a}$$

$$\dot{\boldsymbol{\epsilon}} = \frac{1}{2}\left[\eta\mathbf{1} + \boldsymbol{\epsilon}^{\times}\right]\boldsymbol{\omega}_{ob}^b \tag{9b}$$

B. Dynamics

The equations of motion for a L-wheel gyrostat can be written as

$$\dot{\mathbf{h}}_b = \boldsymbol{\tau}_e - \left[\mathbf{J}^{-1}(\mathbf{h}_b - \boldsymbol{\Lambda}\mathbf{h}_a)\right] \times \mathbf{h}_b \quad (10a)$$

$$\dot{\mathbf{h}}_a = \boldsymbol{\tau}_a \quad (10b)$$

where $\mathbf{h}_a$ is the $L \times 1$ vector of the axial angular momenta of the wheels, $\boldsymbol{\tau}_e$ is the 3×1 vector of the external torque acting on the body, not including wheel torques, $\boldsymbol{\tau}_a$ is the $L \times 1$ vector of the internal axial torques applied by the platform to the wheels, and $\boldsymbol{\Lambda}$ is the $3 \times L$ matrix whose columns contain the axial unit vectors of the L momentum exchange wheels. Let $\boldsymbol{\omega}_{ib}^b$ denote the angular velocity of the body frame $\mathcal{F}_b$ relative to an inertial frame $\mathcal{F}_i$, measured in $\mathcal{F}_b$. Then, the vector $\mathbf{h}_b$ is the total angular momentum of the spacecraft in the body frame, given as

$$\mathbf{h}_b = \mathbf{J}\boldsymbol{\omega}_{ib}^b + \boldsymbol{\Lambda}\mathbf{h}_a \quad (11)$$

where $\mathbf{J}$ is the inertia-like matrix defined as

$$\mathbf{J} \triangleq \mathbf{I} - \boldsymbol{\Lambda}\mathbf{I}_s\boldsymbol{\Lambda}^{\mathrm{T}} \quad (12)$$

The matrix $\mathbf{I}$ is the inertia of the spacecraft, including wheels, and the matrix $\mathbf{I}_s = \mathrm{diag}\{\mathrm{I}_{s1}, \mathrm{I}_{s2}, ..., \mathrm{I}_{sL}\}$ contains the axial moments of inertia of the wheels. The axial angular momenta of the wheels can be written in terms of the body angular velocity and the axial angular velocities of the wheels relative to the body, $\boldsymbol{\omega}_s$, as

$$\mathbf{h}_a = \mathbf{I}_s\boldsymbol{\Lambda}^{\mathrm{T}}\boldsymbol{\omega}_{ib}^b + \mathbf{I}_s\boldsymbol{\omega}_s \quad (13)$$

Note that $\boldsymbol{\omega}_s = [\boldsymbol{\omega}_{s1}, \boldsymbol{\omega}_{s2}, ..., \boldsymbol{\omega}_{sL}]^{\mathrm{T}}$ is an $L \times 1$ vector, and that these relative angular velocities are those that would for instance be measured by tachometers fixed to the platform.

Equation (10) can also be written in terms of angular velocities. By defining $\boldsymbol{\mu} \triangleq [\mathbf{h}_b, \mathbf{h}_a]^{\mathrm{T}}$ and $\boldsymbol{\upsilon} \triangleq [\boldsymbol{\omega}_{ib}^b, \boldsymbol{\omega}_s]^{\mathrm{T}}$ we can write (11) and (13) in the compact form

$$\boldsymbol{\mu} = \boldsymbol{\Gamma}\,\boldsymbol{\upsilon}, \quad \text{where } \boldsymbol{\Gamma} = \begin{bmatrix} \mathbf{I} & \boldsymbol{\Lambda}\mathbf{I}_s \\ \mathbf{I}_s\boldsymbol{\Lambda}^{\mathrm{T}} & \mathbf{I}_s \end{bmatrix} \quad (14)$$

Clearly, we can find $\boldsymbol{\omega}_{ib}^b$ and $\boldsymbol{\omega}_s$ from $\boldsymbol{\upsilon} = \boldsymbol{\Gamma}^{-1}\boldsymbol{\mu}$, or equally, we can write $\dot{\boldsymbol{\upsilon}} = \boldsymbol{\Gamma}^{-1}\dot{\boldsymbol{\mu}}$. By utilizing the matrix inversion lemma, together with (14), we get that

$$\begin{bmatrix} \dot{\boldsymbol{\omega}}_{ib}^b \\ \dot{\boldsymbol{\omega}}_s \end{bmatrix} = \begin{bmatrix} \mathbf{J}^{-1} & -\mathbf{J}^{-1}\boldsymbol{\Lambda} \\ -\boldsymbol{\Lambda}^{\mathrm{T}}\mathbf{J}^{-1} & \boldsymbol{\Lambda}^{\mathrm{T}}\mathbf{J}^{-1}\boldsymbol{\Lambda} + \mathbf{I}_s^{-1} \end{bmatrix} \begin{bmatrix} \dot{\mathbf{h}}_b \\ \dot{\mathbf{h}}_a \end{bmatrix} \quad (15)$$

which can be written as

$$\dot{\boldsymbol{\omega}}_{ib}^b = \mathbf{J}^{-1}\left[-(\boldsymbol{\omega}_{ib}^b)^{\times}(\mathbf{I}\boldsymbol{\omega}_{ib}^b + \boldsymbol{\Lambda}\mathbf{I}_s\boldsymbol{\omega}_s) + \boldsymbol{\tau}_e\right] - \boldsymbol{\Lambda}\boldsymbol{\tau}_a \quad (16a)$$

$$\dot{\boldsymbol{\omega}}_s = \boldsymbol{\Lambda}^{\mathrm{T}}\mathbf{J}^{-1}\left[(\boldsymbol{\omega}_{ib}^b)^{\times}(\mathbf{I}\boldsymbol{\omega}_{ib}^b + \boldsymbol{\Lambda}\mathbf{I}_s\boldsymbol{\omega}_s) - \boldsymbol{\tau}_e\right] + \left[\boldsymbol{\Lambda}^{\mathrm{T}}\mathbf{J}^{-1}\boldsymbol{\Lambda} + \mathbf{I}_s^{-1}\right]\boldsymbol{\tau}_a \quad (16b)$$

As can be seen from (16), the angular velocities are given in $\mathcal{F}_b$ relative to $\mathcal{F}_i$, while the kinematics in (9) are relative to $\mathcal{F}_o$. However, it would be preferable if we in the model could represent the attitude of $\mathcal{F}_b$ relative to $\mathcal{F}_o$. This can be done by utilizing the relation

$$\boldsymbol{\omega}_{ib}^b = \boldsymbol{\omega}_{ob}^b + \mathbf{R}_o^b\boldsymbol{\omega}_{io}^o \quad \text{and} \quad \dot{\boldsymbol{\omega}}_{ib}^b = \dot{\boldsymbol{\omega}}_{ob}^b + \dot{\mathbf{R}}_o^b\boldsymbol{\omega}_{io}^o \quad (17)$$

where $\boldsymbol{\omega}_{io}^o = [0, -\omega_0, 0]^{\mathrm{T}}$, and ω_0 is assumed constant and equal to the mean angular velocity of $\mathcal{F}_o$, given in $\mathcal{F}_i$. This implies circular orbits. For the remainder, we let $\mathbf{c}_i$ denote the i'th column of the rotation matrix $\mathbf{R}_o^b$. We also include the gravity gradient as a disturbance, that is $\boldsymbol{\tau}_e = \boldsymbol{\tau} + \boldsymbol{\tau}_g$, where $\boldsymbol{\tau}$ is the torque provided from thrusters, while the gravity gradient is given as

$$\boldsymbol{\tau}_g = 3\omega_0^2\left[\mathbf{c}_3 \times (\mathbf{I}\mathbf{c}_3)\right]. \quad (18)$$

By utilizing (8) and (17), we can rewrite (16) as

$$\dot{\boldsymbol{\omega}}_{ob}^b = \hat{f}_{inert} + \hat{f}_{\tau} + \hat{f}_g + \hat{f}_{add} \quad (19a)$$

$$\dot{\boldsymbol{\omega}}_s = \bar{f}_{inert} + \bar{f}_{\tau} + \bar{f}_g \quad (19b)$$

where

$$\begin{aligned}
\hat{f}_{inert} &= \mathbf{J}^{-1}\left[-(\boldsymbol{\omega}_{ob}^b - \omega_o\mathbf{c}_2)^{\times} \left(\mathbf{I}\left[\boldsymbol{\omega}_{ob}^b - \omega_o\mathbf{c}_2\right] + \boldsymbol{\Lambda}\mathbf{I}_s\boldsymbol{\omega}_s\right)\right] \\
\bar{f}_{inert} &= \boldsymbol{\Lambda}^{\mathrm{T}}\mathbf{J}^{-1}\left[(\boldsymbol{\omega}_{ob}^b - \omega_o\mathbf{c}_2)^{\times} \left(\mathbf{I}\left[\boldsymbol{\omega}_{ob}^b - \omega_o\mathbf{c}_2\right] + \boldsymbol{\Lambda}\mathbf{I}_s\boldsymbol{\omega}_s\right)\right] \\
\hat{f}_{\tau} &= \mathbf{J}^{-1}\boldsymbol{\tau} - \mathbf{J}^{-1}\boldsymbol{\Lambda}\boldsymbol{\tau}_a \\
\bar{f}_{\tau} &= -\boldsymbol{\Lambda}^{\mathrm{T}}\mathbf{J}^{-1}\boldsymbol{\tau} + \left[\boldsymbol{\Lambda}^{\mathrm{T}}\mathbf{J}^{-1}\boldsymbol{\Lambda} + \mathbf{I}_s^{-1}\right]\boldsymbol{\tau}_a \\
\hat{f}_g &= \mathbf{J}^{-1}\left[3\omega_0^2\mathbf{c}_3 \times (\mathbf{I}\mathbf{c}_3)\right] \\
\bar{f}_g &= -\boldsymbol{\Lambda}^{\mathrm{T}}\mathbf{J}^{-1}\left[3\omega_0^2\mathbf{c}_3 \times (\mathbf{I}\mathbf{c}_3)\right] \\
\hat{f}_{add} &= \omega_o\dot{\mathbf{c}}_2
\end{aligned}$$

III. ATTITUDE CONTROL BY MEANS OF EXPLICIT MPC

In the following, the explicit MPC controller is computed based on the work and algorithms in [15], and some aspects considering implementation are discussed.

The complete nonlinear model (9) and (19) is written as

$$\dot{\mathbf{x}} = \mathbf{f}(\mathbf{x}, \mathbf{u}) = [\dot{\boldsymbol{\omega}}_{ob}^b, \dot{\boldsymbol{\omega}}_s, \dot{\eta}, \dot{\boldsymbol{\epsilon}}]^{\mathrm{T}} \quad (20)$$

where $\boldsymbol{\omega}_{ob}^b \triangleq [\omega_1, \omega_2, \omega_3]^{\mathrm{T}}$, $\boldsymbol{\omega}_s \triangleq \omega_s$, $\boldsymbol{\epsilon} \triangleq [\epsilon_1, \epsilon_2, \epsilon_3]^{\mathrm{T}}$, and $\mathbf{u} \triangleq [\boldsymbol{\tau}^{\mathrm{T}}, \boldsymbol{\tau}_a^{\mathrm{T}}]^{\mathrm{T}} = [\tau_1, \tau_2, \tau_3, \tau_a]^{\mathrm{T}}$.

A. Explicit MPC controller for the SSETI/ESEO satellite

As we consider a linear MPC approach in this paper, it is necessary to linearize the nonlinear model (20). By choosing the equilibrium point p equal to $\mathbf{x}^p = [\mathbf{0}^4, 1, \mathbf{0}^3]^{\mathrm{T}}$, $\mathbf{u}^p = \mathbf{0}^4$, which equals the scenario where $\mathcal{F}_b$ coincides with $\mathcal{F}_o$ and the angular velocity of the wheel is zero, it can be found that the linearized model can be written as

$$\Delta\dot{\mathbf{x}} = \mathbf{A}_c\Delta\mathbf{x} + \mathbf{B}_c\Delta\mathbf{u} \quad (21)$$

where the matrices $\mathbf{A}_c$ and $\mathbf{B}_c$ are given as

$$\mathbf{A}_c = \begin{bmatrix} 0 & 0 & (1-k_x)\omega_0 & 0 \\ 0 & 0 & 0 & 0 \\ (k_z-1)\omega_0 & 0 & 0 & 0 \\ 0 & 0 & 0 & 0 \\ 0 & 0 & 0 & 0 \\ \frac{1}{2} & 0 & 0 & 0 \\ 0 & \frac{1}{2} & 0 & 0 \\ 0 & 0 & \frac{1}{2} & 0 \end{bmatrix} \begin{bmatrix} 0 & -8k_x\,\omega_0^2 & 0 & 0 \\ 0 & 0 & \frac{-6\,k_y i_{22}\,\omega_0^2}{\kappa} & 0 \\ 0 & 0 & 0 & -2k_z\omega_0^2 \\ 0 & 0 & \frac{6\,k_y i_{22}\,\omega_0^2}{\kappa} & 0 \\ 0 & 0 & 0 & 0 \\ 0 & 0 & 0 & 0 \\ 0 & 0 & 0 & 0 \\ 0 & 0 & 0 & 0 \end{bmatrix} \quad (22a)$$

$$\mathbf{B}_c = \begin{bmatrix} \frac{1}{i_{11}} & 0 & 0 & 0 \\ 0 & \frac{1}{\kappa} & 0 & -\frac{1}{\kappa} \\ 0 & 0 & \frac{1}{i_{33}} & 0 \\ 0 & -\frac{1}{\kappa} & 0 & \frac{i_{22}}{\kappa\,\mathrm{I}_s} \\ 0 & 0 & 0 & 0 \\ 0 & 0 & 0 & 0 \\ 0 & 0 & 0 & 0 \\ 0 & 0 & 0 & 0 \end{bmatrix} \quad (22b)$$

where we used $\mathbf{I} = \mathrm{diag}(i_{11}, i_{22}, i_{33})$, $k_x = \frac{i_{22}-i_{33}}{i_{11}}$, $k_y = \frac{i_{11}-i_{33}}{i_{22}}$, $k_z = \frac{i_{22}-i_{11}}{i_{33}}$, and $\kappa = i_{22} - \mathrm{I}_s$ for short.

From the system matrix in (22a), we immediately conclude that the linearized system is uncontrollable, as the terms corresponding to the state η equal zero. However, the linearized system is found to be stabilizable, and omitting η, also controllable. Also note that we can utilize the fact that the Euler parameters satisfy $\eta^2 + \boldsymbol{\epsilon}^{\mathrm{T}}\boldsymbol{\epsilon} = 1$, making us able to keep track of, and update η in an open-loop manner.

Before we can apply the mpQP algorithm, (21) is converted into an equivalent *discrete-time* form by utilizing a modified first-order hold approach. The sampling time is chosen as $\mathrm{T}_s = 0.1$ [sec], and when deriving the controller, η is omitted, introducing the new state vector $\widetilde{\mathbf{x}} \in \mathbb{R}^7$.

TABLE II

SUMMARY OF TUNING PARAMETERS

Parameter	Value
$\mathbf{Q}$	$\mathrm{diag}\{200, 200, 200, 5\cdot 10^{-7}, 1, 1, 1\}$
$\mathbf{R}$	$\mathrm{diag}\{100, 200, 100, 1\}$
N (horizon)	2
$\boldsymbol{\rho}$ (slack)	$8\cdot 10^{-5}$

The tuning parameters used for deriving the explicit MPC controller are summarized in Table II. Furthermore, the parameter space, in which solve the mpQP, is chosen as

$$-[1,1,1,1000,1,1,1]^{\mathrm{T}} \leq \widetilde{\mathbf{x}} \leq [1,1,1,1000,1,1,1]^{\mathrm{T}} \quad (23)$$

while the desirable constraints are given as

$$\mathbf{u}_{max} = -\mathbf{u}_{min} = \begin{bmatrix} 0.0484 \\ 0.0484 \\ 0.0398 \\ 0.0020 \end{bmatrix}, \quad |\omega_s| \leq 527. \quad (24)$$

The constraints on $\mathbf{u}$ are chosen based on the nominal thruster torques and maximum wheel torque, given in Table I, while the constraint on the wheel angular velocity was defined by the SSETI project due to power consumption.

The solution of the mpQP, obtained from the discrete-time version of (21), Table I and II, and (24), gives a polyhedral partition over the parameter space in (23), consisting of 2867 regions. If we denote each of these polyhedra as $\mathcal{X}_i$, where i is the specific region, then $\mathcal{X}_i \subset \mathbb{R}^7$. Examples of planar intersections are shown in Fig. 1. Each polyhedron contains an optimal control law such that if $\widetilde{\mathbf{x}}(k) \in \mathcal{X}_i$ then

$$\mathbf{u}(k) = \mathbf{K}_i\widetilde{\mathbf{x}}(k) + \mathbf{k}_i. \quad (25)$$

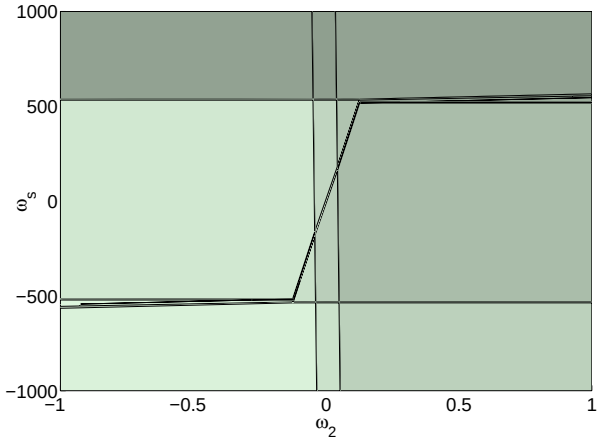

(a) $\omega_2\omega_s$-plane

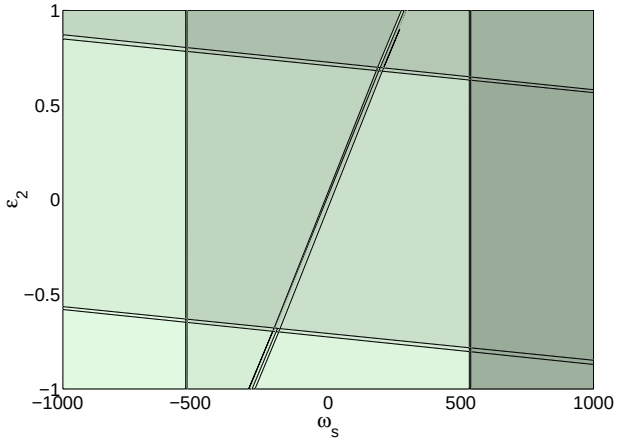

(b) $\omega_s\epsilon_2$-plane

Fig. 1. Polyhedral partition, $N = 2$ and $\boldsymbol{\rho} = 8\cdot 10^{-5}$

B. Bang-bang modulation

A bang-bang modulation scheme can be applied for dealing with the on-off nature of the actuating thrusters. The technique is best explained through Fig. 2, where $\mathbf{K}_{nom}$ is the nominal thruster torques, and $\mathbf{u}_*$ is given according to

$$\mathbf{u}_* : \text{sign}(\mathbf{u}) = \begin{cases} -\mathbf{1} & \text{if } \mathbf{u} \leq -dz, \\ \mathbf{1} & \text{if } \mathbf{u} \geq dz. \end{cases} \tag{26}$$

Other techniques also exist in solving this problem, one being pulse-with pulse-frequency (PWPF) modulation [6].

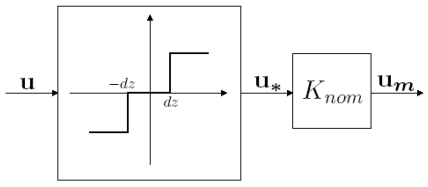

Fig. 2. Bang-bang modulation with dead-zone

IV. Simulations

The closed-loop simulations in this section have been performed with the complete nonlinear model (20), where initial conditions for the dynamics and kinematics, as well as initial Keplerian orbital elements, are given in Table III.

Usually control requirements for a satellite are specified according to the diversified situations it is expected to face during its lifetime. However, only the *nominal* mode will be considered at this point, which means that the best obtainable result is whenever the body frame $\mathcal{F}_b$ coincides with the orbit frame $\mathcal{F}_o$.

In the plots the Euler parameters have been transformed into Euler angles [deg].

A. Case I

No noise is present in this case, and the bang-bang modulation is not applied. The results are given in Fig. 3, and as can be seen, the state trajectories converge to zero while keeping actuation and states within their constraints.

B. Case II

Similar scenario as in Case I, but also including measurement noise according to Table IV. Bang-bang modulation is used for realizing the on-off nature of the thrusters, where the dead-zone, $\mathbf{dz}$, is chosen based on performance as well as fuel consumption. The results are given in Fig. 4. As in Case I, we obtain a desired behavior while none of the constraints are violated.

V. CONCLUSIONS

It has been shown that explicit solutions to constrained linear MPC problems can be computed for the attitude control problem by solving multi-parametric quadratic programs (mpQP). Through theory and simulations the approach has shown to be highly potential, and it should be considered if constraints need to be taken into account.

TABLE III

SUMMARY OF SIMULATIONS

Case I and II	**Initial condition**	**Set-point**	**Unit**
$\boldsymbol{\omega}_{ob}^b$	$\{-0.05, 0.15, -0.08\}$	$\{0, 0, 0\}$	rad/s
ω_s	400	0	rad/s
Euler angles (XYZ)	$\{-25, 60, 90\}$	$\{0, 0, 0\}$	deg
Keplerian elements	**Initial condition**		**Unit**
$[i, \omega, \Omega, \nu]$	$\{7, 178, -10, 0\}$		deg
a	17125		km
e	0.0		-

TABLE IV

RMS ERRORS IN STATES

States	**Errors**	**Unit**
$\boldsymbol{\omega}_{ob}^b$	$\{0.0035, 0.0052, 0.0035\}$	rad/s
ω_s	0.5	rad/s
Euler angles (XYZ)	$\{0.1, 0.1, 0.1\}$	deg

References

[1] Hegrenæs Ø., "Attitude Control by means of Explicit Model Predictive Control, via Multi-parametric Quadratic Programming", *MSc. thesis*, Norwegian University of Science and technology, (2004).

[2] Tsiotras P., "New Control Laws for the Attitude Stabilization of Rigid Bodies", *13th IFAC Symposium on Automatic Control in Aerospace*, (1994).

[3] Hall, C. D., P. Tsiotras and H. Shen, "Tracking Rigid Body Motion Using Thrusters and Momentum Wheels", *The Journal of the Astronautical Sciences*, Vol. 50, No. 3, pp. 311-323, (2002).

[4] Cavallo, A. and G. De Maria, "Attitude control for large angle maneuvers", *IEEE International Workshop*, pp. 232-237,(1996).

[5] Chen, Y-P. and S-C. Lo, "Sliding-mode controller design for spacecraft attitude tracking maneuvers", *IEEE Transactions on Aerospace and Electronic Systems*, Vol. 29, no. 4, pp. 1328-1333, (1993).

[6] Wie, B. and P. M. Barba, "Quaternion feedback for spacecraft large angle maneuvers", *Journal of Guidance, Control, and Dynamics*, Vol. 8, no. 3, pp. 360-365, (1985).

[7] Joshi, S. M., A. G. Kelkar and J. T.-Y. Wen, "Robust attitude stabilization of spacecraft using nonlinear quaternion feedback", *IEEE Transactions on Automatic Control*, Vol. 40, no. 10, pp. 1800-1803, (1995).

[8] Singh S. N.,"Nonlinear Adaptive Attitude Control for Spacecraft", *IEEE Transactions on Aerospace and Electronic Systems*, Vol. 23, no. 3, pp. 371-380, (1987).

[9] Show, L.-L., J.-C. Juang and C.-D. Yang, "Nonlinear $\mathcal{H}_\infty$ robust control for satellite large angle attitude maneuvers", *ACC*, Vol. 2, pp. 1357-1362, (2001).

[10] Dalsmo, M. and O. Egeland, "State feedback $\mathcal{H}_\infty$ control of a rigid spacecraft", *Proceedings of the 34th IEEE Conference on Decision and Control*, Vol. 4, pp. 3968-3973, (1995).

[11] Sun, Y.-P. and C.-D. Yang, "Mixed $\mathcal{H}_2/\mathcal{H}_\infty$ attitude control of a LEO microsatellite in the presence of inertia matrix uncertainty", *ACC*, Vol. 2, pp. 1354-1359, (2002).

[12] Show, L.-L., J.-C. Juang, C.-T. Lin and Y.-W. Jan, "Spacecraft robust attitude tracking design: PID control approach", *Proceedings of the ACC*, Vol. 2, pp. 1360-1365, (2002).

[13] Ferrari-Trecate, G., F. A. Cuzzola, D. Mignone and M. Morari, "Analysis and control with performance of piecewise affine and hybrid systems", *ACC*, Vol. 1, pp. 200-205, (2001).

[14] Bemporad, A., M. Morari, V. Dua and E. N. Pistikopoulos, "The explicit linear quadratic regulator for constrained systems", *Automatica*, Vol. 38, pp. 3-20, (2002).

[15] Tøndel, P., T. A. Johansen and A. Bemporad, "An algorithm for multiparametric quadratic programming and explicit MPC solutions", *Automatica*, Vol. 39, pp. 489-497, (2003).

[16] Hughes, P. C., "Spacecraft attitude dynamics", *John Wiley & Sons*, (1986).

[17] Egeland, O. and J. T. Gravdahl, "Modeling and Simulation for Automatic Control", *Marine Cybernetics, Trondheim, Norway*, (2002).

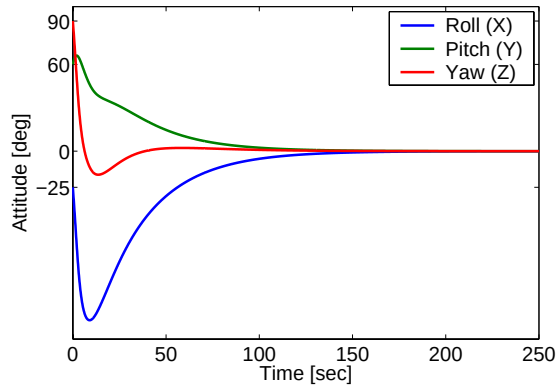

(a) Euler angles

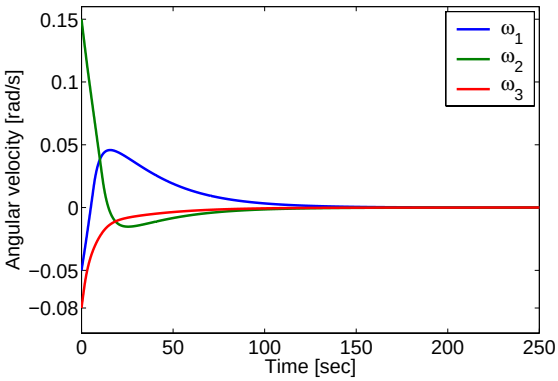

(b) Angular velocity

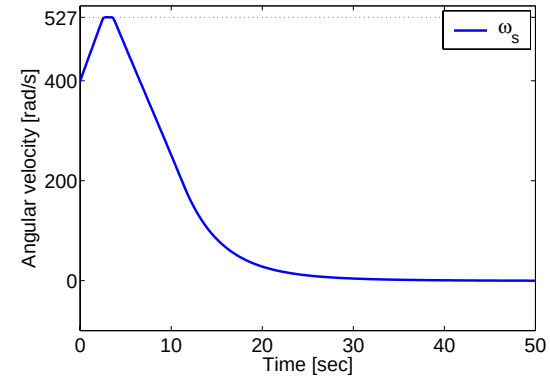

(c) Wheel velocity (magnified)

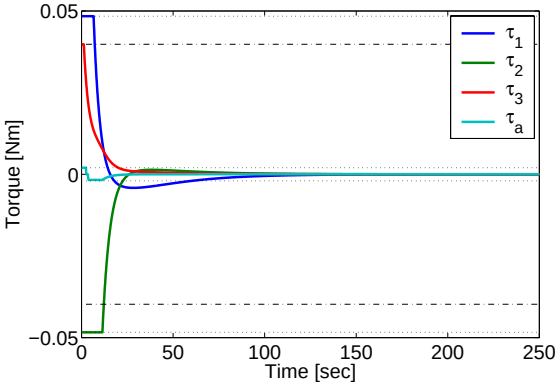

(d) Input torques

Fig. 3. Case I, $N = 2$ and $\boldsymbol{\rho} = 8 \cdot 10^{-5}$

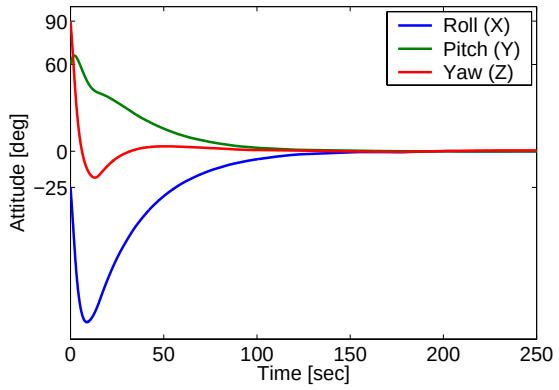

(a) Euler angles

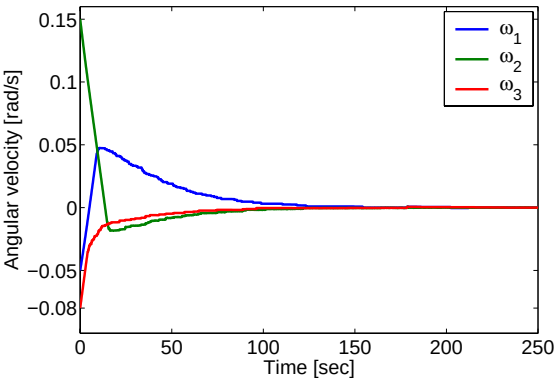

(b) Angular velocity

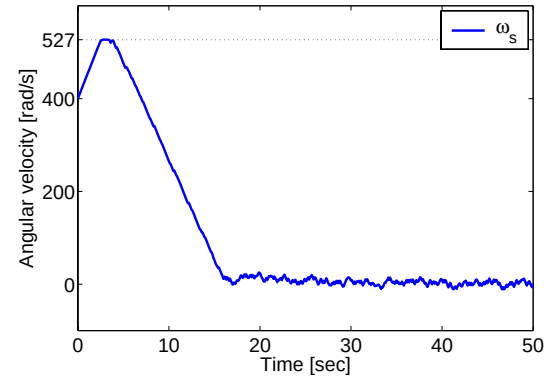

(c) Wheel velocity (magnified)

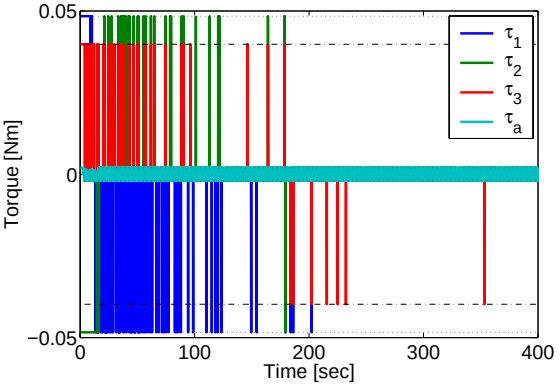

(d) Input torques (expanded)

Fig. 4. Case II, $N = 2$ and $\boldsymbol{\rho} = 8 \cdot 10^{-5}$